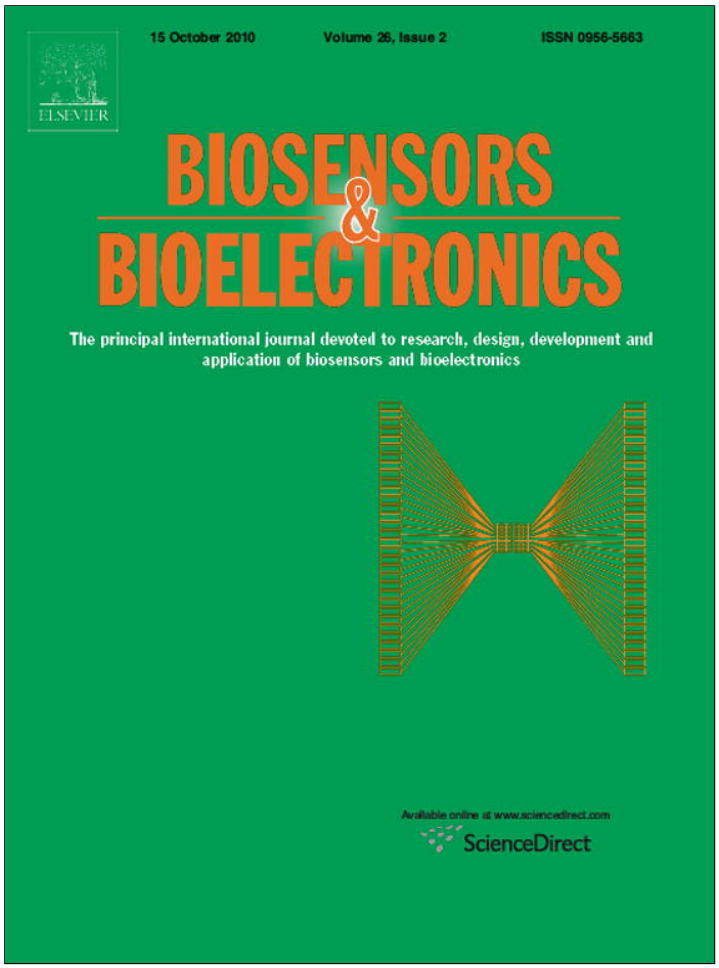

Biosensors and Bioelectronics 26 (2010) 549–554

Contents lists available at ScienceDirect

Biosensors and Bioelectronics

journal homepage: www.elsevier.com/locate/bios

Layer-by-layer assembly of bi-protein/layered double hydroxide ultrathin film and its electrocatalytic behavior for catechol

Xianggui Kong, Xiuying Rao, Jingbin Han, Min Wei*, Xue Duan

State Key Laboratory of Chemical Resource Engineering, Beijing University of Chemical Technology, Beijing 100029, China

ARTICLE INFO

Article history:
Received 16 May 2010
Received in revised form 11 July 2010
Accepted 12 July 2010
Available online 17 July 2010

Keywords:
LBL assembly
Layered double hydroxides
Bi-protein electrode
Biosensor

ABSTRACT

This paper reports the fabrication of a bi-protein/layered double hydroxide (LDH) ultrathin film in which hemoglobin (HB) and horseradish peroxidase (HRP) molecules were assembled alternately with LDH nanosheets *via* the layer-by-layer (LBL) deposition technique, and its electrocatalytic performances for oxidation of catechol were demonstrated. The results of XRD indicate that the HB–HRP/LDH ultrathin film possesses a long range stacking order in the normal direction of the substrate, with the two proteins accommodated in the LDH gallery respectively as monolayer arrangement. SEM images show that the film surface exhibits a continuous and uniform morphology, and AFM reveals the Root-Mean-Square (RMS) roughness of ~10.2 nm for the film. A stable direct electrochemical redox behavior of the proteins was successfully obtained for the HB–HRP/LDH film modified electrode. In addition, it exhibits remarkable electrocatalytic activity towards oxidation of catechol, based on the synergistic effect of the two proteins. The catechol biosensor in this work displays a wide linear response range (6–170 μM, $r = 0.999$), low detection limit (5 μM), high sensitivity and good reproducibility.

1. Introduction

Recently, the third generation biosensors based on direct electrochemistry of redox proteins have received extensive attention, for the purpose of obtaining high performing catalyst with high efficiency and selectivity (Cao et al., 2008; Zeng et al., 2009; Xiong et al., 2007; Liu et al., 2005). The main driving force for this enhanced activity is the increasing demand for miniaturized biosensors, particularly for medical diagnostics and environmental analysis applications. However, proteins are inclined to lose their electrochemical activity and bioactivity when directly adsorbed or immobilized onto an electrode surface. Therefore, to select a host matrix which can both provide a suitable microenvironment for proteins and enhance direct electron transfer between proteins and underlying electrodes is one of the main challenges in this field (Chen et al., 2008). As a result, a large number of organic and inorganic materials, such as polymers (Lu et al., 2006; Shutava et al., 2006; Shi et al., 2003; Zhao et al., 2005), layered clays (Zhou et al., 2007; Mousty et al., 2008; Maaref et al., 2007), nanomaterials (Kim et al., 2008; Luo et al., 2009; Zhu et al., 2009; Delvaux et al., 2005) and mesoporous matrices (Zhang et al., 2007; Tortajada et al., 2005; Sun et al., 2006), have been employed as supports to improve the biosensor performance. Among the materials mentioned above, layered materials are very attractive for the immobilization of proteins due to their specific 2D structure, low cost, high stability and large surface-to-volume ratio (Chen et al., 2007; Macha and Fitch, 1998).

Layered double hydroxides (LDHs, represented as $[M^{II}_{1-x}M^{III}_{x}(OH)_2]^{x+}(A^{n-})_{x/n}\cdot mH_2O$) are one family of anionic clays consisting of positively charged brucite-like layers and exchangeable interlayer anions (Williams and O'Hare, 2006; Leroux et al., 2003; Fogg et al., 1999, 2002; Boclair and Braterman, 1999). Based on the 2D structure, unique ion-exchange properties as well as good biocompatibility, LDH materials have been widely used as host matrices for the storage and release of biomolecules (Khan et al., 2001; Xu and Braterman, 2007; Geraud et al., 2008; Leroux et al., 2004). However, further applications are largely restricted because most of biomolecules can only be adsorbed on the surface of LDH particles due to their large size, resulting in low loading and serious aggregation. Recently, the delamination of LDH to single nanosheet as building block and preparation of inorganic/organic ultrathin films (UTFs) have been reported (Li et al., 2005; Ma et al., 2007; Yan et al., 2009). This inspires us to challenge the goal of fabricating electrochemical biosensors through alternate assembly of positively charged LDH nanosheets and negatively charged protein *via* the layer-by-layer (LBL) technique. The resulting UTFs would exhibit the following advantages: firstly, the LDH nanosheets can provide a confined and stable microenvironment for the immobilization of protein molecules; secondly, the molecular level control of the assembly will result

* Corresponding author. Tel.: +86 10 64412131; fax: +86 10 64425385.
E-mail addresses: weimin@mail.buct.edu.cn, weimin-hewei@163.com (M. Wei).

0956-5663/$ – see front matter © 2010 Elsevier B.V. All rights reserved.
doi:10.1016/j.bios.2010.07.045

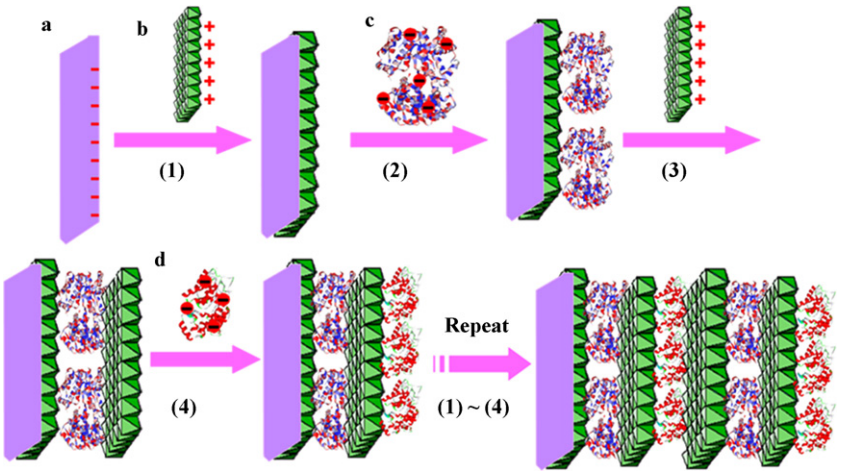

Scheme 1. Schematic representation of the process for the fabrication of $(LDH/HB/LDH/HRP)_n$ modified electrode: (a) pretreated ITO electrode, (b) Ni–Al-LDH nanosheet, (c) HB anion, and (d) HRP anion.

in a high dispersion of protein with uniform orientation, which facilitates the electron transfer. Moreover, the film component and thickness can be precisely controlled at nanometer scale with simple manipulation and versatility.

In this work, we report the fabrication of a novel bi-proteinic electrode based on (LDH nanosheet/hemoglobin/LDH nanosheet/horseradish peroxidase)$_n$ UTFs through the electrostatic LBL assembly. Herein, the positively charged Ni–Al-LDH nanosheets as building blocks were assembled alternately with two negatively charged heme-containing proteins (hemoglobin (HB) and horseradish peroxidase (HRP)) on an indium–tin oxide-coated glass (ITO) substrate (Scheme 1). The structural and morphological studies show that the UTF is continuous and uniform with long range stacking order in the normal direction of the substrate, and the two protein molecules are accommodated respectively in the LDH gallery as monolayer arrangement. The UTF modified electrode exhibits a stable direct electrochemical behavior owing to the redox of biomolecules; moreover, it shows remarkable electrocatalytic activity towards oxidation of catechol without involvement of H_2O_2, based on the synergistic effect of the two proteins. The bi-proteinic electrode displays a wide linear response range, low detection limit, high sensitivity and good reproducibility. Therefore, this work provides a novel and efficient strategy for the immobilization of bioactive proteins into an inorganic layered matrix, for the purpose of potential applications in electroanalysis and biosensor.

2. Experimental

2.1. Materials and reagents

The hemoglobin (HB, pI = 6.8) was purchased from Worthington Biochemical Corporation. Horseradish peroxidase (HRP, 250 U mg^{-1}, pI = 7.2) and polyetherimide (PEI, MW = 50,000) were obtained from Sigma Chemical Co. Ltd. Poly(styrene sulfonic acid) (PSS, MW = 70,000) was purchased from Alfa Aesar Chemical Co. Ltd. All other chemicals were of analytical grade and used as received without further purification. The aqueous solutions in all the experiments were prepared with Milli-Q water.

2.2. Preparation of Ni–Al-LDH nanosheets

The Ni–Al-LDH nanosheet was prepared according to the reported method (Han et al., 2008). In a typical procedure, $Ni(NO_3)_2{\cdot}6H_2O$ (10 mmol), $Al(NO_3)_3{\cdot}9H_2O$ (5 mmol) and urea (15 mmol) were dissolved in 100 mL of deionized water, sealed in an autoclave and heated at 190 °C for 48 h. The resulting product was filtered, washed thoroughly with deionized water and anhydrous ethanol and then dried in vacuum at 60 °C for 24 h. 0.1 g of this sample was vigorously agitated in 100 mL of formamide under a N_2 flow at room temperature for 48 h. The formamide was used as solvent to swell and exfoliate the LDH particles. The exfoliation of LDH particles in formamide was a facile method to obtain LDH single nanosheets without the need of heating or refluxing treatment (Ma et al., 2006; Liu et al., 2006). After these procedures, a colloidal suspension of unilamellar, positively charged Ni–Al-LDH nanosheets was obtained.

2.3. Assembly of $(LDH/HB/LDH/HRP)_n$ UTFs

Prior to assembly, ITO substrates (3.0 cm × 1.0 cm) were cleaned by sonication in a series of solvents: acetone, ethanol and deionized water for 10 min each time. Quartz glass (3.0 cm × 1.0 cm) substrates were cleaned by immersing in a fresh piranha solution (H_2SO_4:H_2O_2 (30%) = 3:1, v/v) (warning: piranha solution is very corrosive and must be treated with extreme care) for about 40 min, followed by rinsing in deionized water and drying with a N_2 flow. The cleaned ITO and quartz substrates were firstly dipped into a cationic PEI solution (1 mg mL^{-1}) and then anionic PSS solution (1 mg mL^{-1}) for 20 min respectively, and then washed thoroughly and dried with a N_2 flow after each deposition. After these processes, the substrates were modified with a PEI/PSS precursor film, resulting in a negatively charged surface.

The fabrication of the $(LDH/HB/LDH/HRP)_n$ UTFs were carried out by alternate immersion of the PEI/PSS coated substrates in LDH nanosheets colloidal suspension, HB solution (1 mg mL^{-1} in 0.1 M PBS, pH = 8.0), LDH nanosheets colloidal and HRP solution (1 mg mL^{-1} in 0.1 M PBS, pH = 8.0) respectively, for 15 min each time. Water rinsing and N_2 drying were performed after each deposition step. Similarly, the respective $(LDH/HB/LDH/HB)_n$ and $(LDH/HRP/LDH/HRP)_n$ UTF modified ITO electrodes were also prepared for comparison. The resulting films were finally rinsed, dried and stored in 4 °C before use.

2.4. Characterization and amperometric measurements

UV–vis absorption spectra were recorded using a Shimadzu UV-2501PC spectrometer after each deposition cycle for the purpose of monitoring the growth of UTF. XRD patterns of the $(LDH/HB/LDH/HRP)_n$ films were recorded using a Rigaku

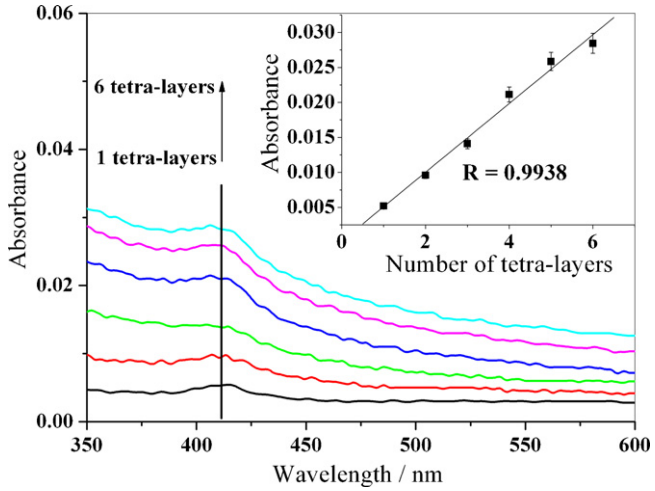

Fig. 1. UV–vis absorption spectra of the $(LDH/HB/LDH/HRP)_n$ UTFs with tetra-layer number (n) ranging in 1–6. The inset displays the linear relationship between the absorbance at 410 nm *vs.* n.

2500VB2+PC diffractometer under the conditions: 40 kV, 50 mA, Cu Kα radiation with step-scanned in step of 0.04° (2θ) in the range 0.5–10° using a count time of 10 s/step. After the ultrathin film was dried with a N_2 flow, its XRD pattern was obtained by attaching the substrate to the sample platform directly. A Hitachi S-3500 scanning electron microscope (accelerating voltage applied was 10 kV) and a NanoScope IIIa Atomic Force Microscope were used to investigate the surface morphology of the UTFs.

A CHI 660B electrochemical workstation (Shanghai Chenhua Instrument Co., China) was utilized for electrochemical measurements. A conventional three-electrode cell was used, including a modified ITO electrode as the working electrode, a platinum wire as the counter and an Ag/AgCl (3 M KCl) as the reference electrode. The solutions were prepared with Milli-Q water (>18 MΩ cm) and purged with highly purified nitrogen for at last 10 min prior to measurement, and a nitrogen atmosphere was maintained during the electrochemical measurements. All measurements were performed at room temperature.

3. Results and discussion

3.1. Structural and morphological characterization of the $(LDH/HB/LDH/HRP)_n$ UTFs

Since the isoelectric point (pI) is 6.8 and 7.2 for HB and HRP respectively, both of them were negatively charged in pH 8.0 PBS and can be used as building blocks for assembly with the positively charged LDH nanosheets *via* electrostatic interaction. Fig. 1 shows the UV–vis spectra of the $(LDH/HB/LDH/HRP)_n$ UTFs on quartz substrate with tetra-layer number n = 1–6, from which a absorption band at ~410 nm attributed to the ferroheme was observed. A red-shift of 5 nm for the UTFs was obtained compared with a mixed HB and HRP solution (Fig. S1), which is possibly related to interactions between protein molecule and LDH nanosheets in the densely packed films. The band intensity at ~410 nm correlates linearly with the increase of n (Fig. 1, inset), indicating a stepwise and uniform film growth procedure.

Fig. 2A shows the small angle XRD patterns of the as-prepared $(LDH/HB/LDH/HRP)_n$ UTFs. A narrow, symmetric and strong Bragg diffraction reflection was observed at 2θ = 0.91°, whose intensity increases gradually upon increasing the tetra-layer number. This diffraction feature can be attributed to a so-called superlattice reflection of the inorganic/organic periodic nanostructure (Liu et al., 2006), indicating the long range stacking order of the films in the normal direction of the substrate. The average thickness of a LDH/HB/LDH/HRP tetra-layer unit is 9.69 nm. By subtracting the thickness of two LDH nanosheets (0.48 × 2 = 0.96 nm, Liu et al., 2006), the gallery height for the summation of HB and HRP in the normal direction is ~8.73 nm. Based on the size of HB (5.0 nm × 5.5 nm × 6.0 nm) and HRP (3.0 nm × 3.5 nm × 6.0 nm), it is proposed that HB and HRP molecules are accommodated respectively as monolayer arrangement between LDH nanosheets.

The successful deposition process of the film on ITO substrates was also demonstrated by the electrochemical impedance spectroscopy (EIS) method (Fig. S2), since EIS is an effective method for studying the impedance changes of the electrode surface during the fabrication process (Shervedani et al., 2006; Shi et al., 2007). The diameter of the Nyquist circle increased with the increase of the tetra-layer number, indicating the augment of electron-transfer resistance along with the deposition procedure. The results above confirm a successful LBL growth of the $(LDH/HB/LDH/HRP)_n$ UTFs on ITO substrates.

The surface morphology of the UTFs was observed by SEM and AFM images. A top-view of SEM image for the $(LDH/HB/LDH/HRP)_3$ film (Fig. 2B) shows that the film surface is continuous and uniform; AFM image (Fig. 2C) reveals that the RMS roughness of the surface is ~10.2 nm. Moreover, the thickness of the films estimated from their side-view SEM images increased linearly with the increase of tetra-layer number (Fig. S3), confirming that the UTFs possess a uniform and periodic layered structure (Yan et al., 2009). The thickness of one tetra-layer unit was calculated to be 9.5 nm from the linear slope (Fig. 2D), in approximately accordance with the result obtained by XRD (9.69 nm).

3.2. Direct electrochemistry of the $(LDH/HB/LDH/HRP)_n$ UTF modified electrode

Cyclic voltammograms (CVs) of different electrodes in 0.1 M PBS (pH = 7.0) is shown in Fig. 3A. No electrochemical response was observed at both the bare ITO electrode (curve a) and the LDH modified electrode (curve b). However, the $(LDH/HB/LDH/HRP)_2$ UTF modified electrode (curve c) gives a couple of well-defined quasi-reversible redox peaks at −0.15 and −0.22 V, respectively. These observations clearly demonstrate that the redox process originates from the reaction of the heme Fe(III)/Fe(II) couple in HB and HRP immobilized in the LBL film. Furthermore, the direct electrochemistry of electrodes modified with different tetra-layer number $(LDH/HB/LDH/HRP)_n$ UTFs was investigated under the same conditions. As shown in Fig. S4, the $(LDH/HB/LDH/HRP)_2$ modified electrode shows better direct electrochemistry behavior compared with the $(LDH/HB/LDH/HRP)_1$ and $(LDH/HB/LDH/HRP)_3$ modified electrode. As a result, the $(LDH/HB/LDH/HRP)_2$ UTF modified electrode was chosen as the working electrode. For comparison, the CV behavior of the $(LDH/HB/LDH/HB)_2$ (Fig. S5A) and $(LDH/HRP/LDH/HRP)_2$ (Fig. S5B) electrode was also investigated. A couple of redox peaks were observed for the two comparison electrodes; however, the peak current is lower than that of the $(LDH/HB/LDH/HRP)_2$ modified electrode.

Fig. 3B shows the CVs of the $(LDH/HB/LDH/HRP)_2$ UTF modified electrode in 0.1 M pH 7.0 PBS at different scan rates. Both the anodic and cathodic peak current increase linearly along with the increase of scan rate in the range 10–100 mV s^{-1} (inset plots in Fig. 3B), indicating a surface-controlled electrochemical process. Moreover, no obvious change in potential was observed for both anodic and cathodic peak upon increasing scan rate, possibly due to the fast electron transfer process between proteins and the electrode surface. The results above suggest that the LDH nanosheets provide proteins with a favorable microenvironment for facilitating electron transfer.

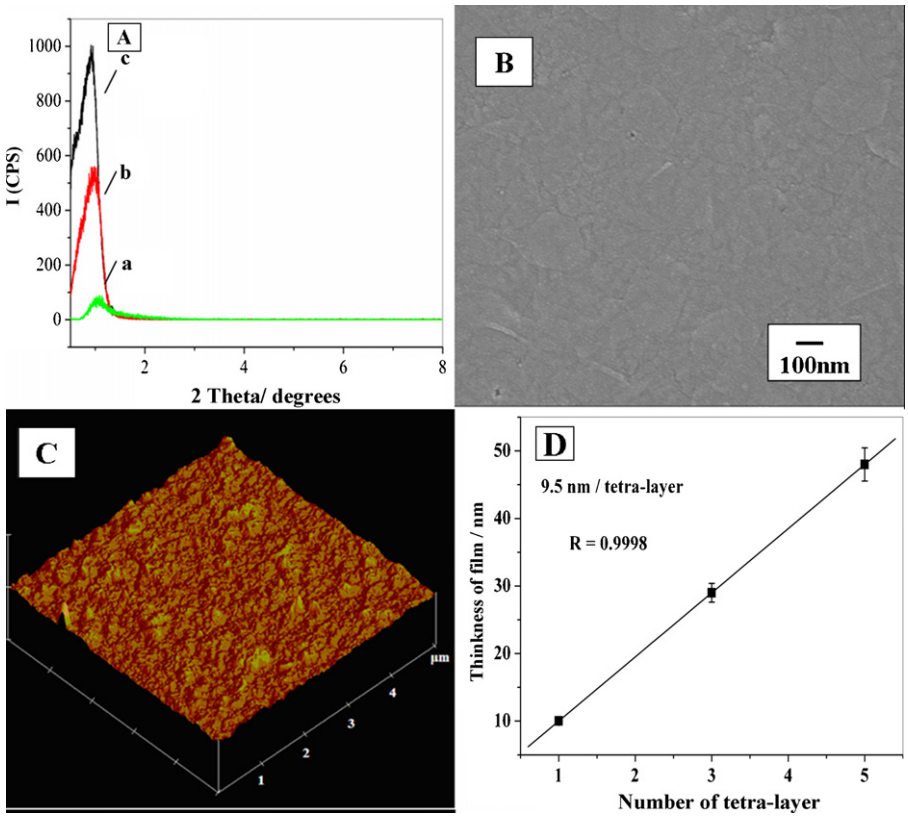

Fig. 2. (A) XRD patterns of the $(LDH/HB/LDH/HRP)_n$ UTFs with different tetra-layers (from a to c, $n = 3, 8, 15$); (B) SEM image of the $(LDH/HB/LDH/HRP)_3$ UTF; (C) AFM image of the $(LDH/HB/LDH/HRP)_3$ UTF; (D) plot of film thickness *vs.* the tetra-layer number.

In addition, the $(LDH/HB/LDH/HRP)_2$ modified electrode shows good stability in 0.1 M pH 7.0 PBS upon consecutive voltammetric sweep over the potential range from −0.8 to 1.1 V. The peak current remains almost unchanged (Fig. 4) after a twice 5-cycle scanning. Furthermore, after the modified electrode was stored at 4 °C for 2 months, the peak current maintained 95% of its initial value. In contrast, the stability studies for the comparison electrodes (Fig. S6) showed that a single protein UTF modified electrode was not as stable as the bi-protein UTF modified electrode. Based on the results above, it can be proposed that a synergistic effect between the two proteins does exist, which might be related to their regular packing and orientation in the LDH nanosheets matrix.

3.3. Electrocatalytic behavior of the $(LDH/HB/LDH/HRP)_2$ UTF modified electrode for catechol

The electrocatalytic oxidation of catechol at the $(LDH/HB/LDH/HRP)_2$ UTF modified electrode was studied by CV measurements (Fig. 5). The cathodic peak current increased while the anodic peak current kept unchanged after the addition of catechol, indicating the electrocatalytic activity of proteins for the oxidation of catechol. However, no obvious electrocatalytic behavior was found for the comparison electrodes modified with $(LDH/HB/LDH/HB)_2$ or $(LDH/HRP/LDH/HRP)_2$ under the same conditions (Fig. S7). This phenomenon further confirms the synergistic

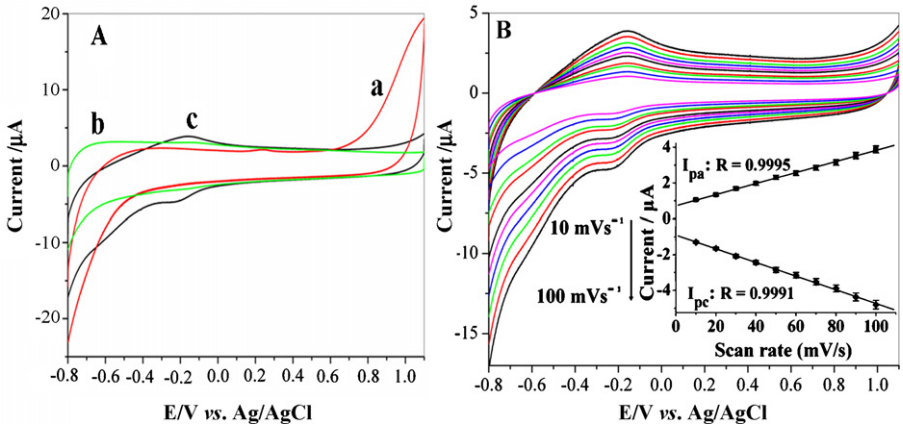

Fig. 3. (A) CVs of (a) bare ITO electrode, (b) LDH nanosheets modified ITO electrode, (c) the $(LDH/HB/LDH/HRP)_2$ UTF modified ITO electrode in 0.1 M pH 7.0 PBS at a scan rate of 100 mV s^{-1}. (B) CVs of the $(LDH/HB/LDH/HRP)_2$ UTF modified electrode in 0.1 M pH 7.0 PBS at different scan rates: 10–100 mV s^{-1}; Inset plots display the peak current *vs.* scan rate.

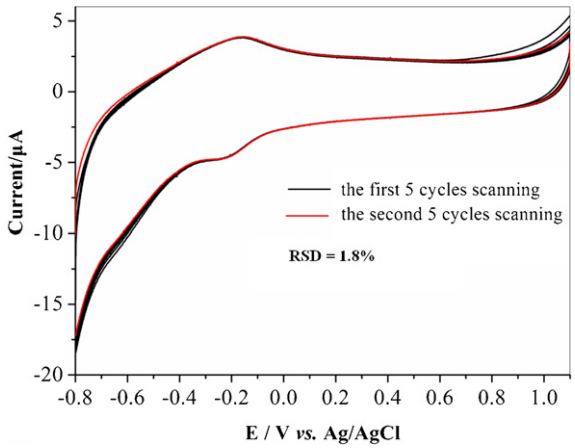

Fig. 4. The stability of $(LDH/HB/LDH/HRP)_2$ UTF modified electrode in 0.1 M pH 7.0 PBS at scan rate of 0.1 V s^{-1}.

effect between the two proteins in this bi-proteinic modified electrode. For the $(LDH/HB/LDH/HRP)_2$ UTF modified electrode, a linear relationship between cathodic peak current and catechol concentration was observed in the concentration range from 6.0×10^{-6} to 1.7×10^{-4} M (inset in Fig. 5). The calibration equation can be expressed as i (μA) = 4.6854 + 0.1312c (μM) with a correlation coefficient of 0.9995, and the detection limit for catechol is 5 μM (S/N = 3). A repetition test of one electrode shows that 90.0% of its initial current remains in 10 consecutive days' measurement. Additionally, the $(LDH/HB/LDH/HRP)_2$ modified electrode exhibits a good reproducibility from the data of five different electrodes with RSD less than 3.0%. Therefore, the $(LDH/HB/LDH/HRP)_2$ modified electrode possesses a wide linear response range, low detection limit, good stability and reproducibility for the determination of catechol.

According to previous reports (Ruzgas et al., 1995; Yang et al., 2006; Marko-Varga et al., 1995), the response of the heme-containing protein biosensors to phenolic compounds is based on a complicated double displacement model in which appropriate content of H_2O_2 regent was involved. Furthermore, the concentration of H_2O_2 significantly affects the performance of the sensor: a high concentration leads to the formation of inactive protein and reduces sensor life; while a low concentration results in weak response signal. However, this drawback was resolved in this bi-proteinic electrode system, for H_2O_2 is not a necessary regent for the oxidation of catechol. Based on the results in this work and the knowledge of literature (Wang et al., 2009), the electrocatalytic behavior of the $(LDH/HB/LDH/HRP)_2$ modified electrode for the oxidation of catechol can be tentatively expressed as follows: as the ferric heme reduces to ferrous heme at the electrode surface, the catechol converts into quinone or free radical product (catechol*), which is electroactive and can be electrochemically reduced at the electrode surface simultaneously. As a result, the cathodic current increases proportionally along with the concentration of phenolic compounds in the solution. According to the results from the mono-protein modified electrode mentioned above, a synergistic interaction between the two proteins originates from their packing and orientation, which plays a key role in facilitating the electron transfer between the electroactive species and the electrode surface. The electrochemical reaction process can be described as the following equations:

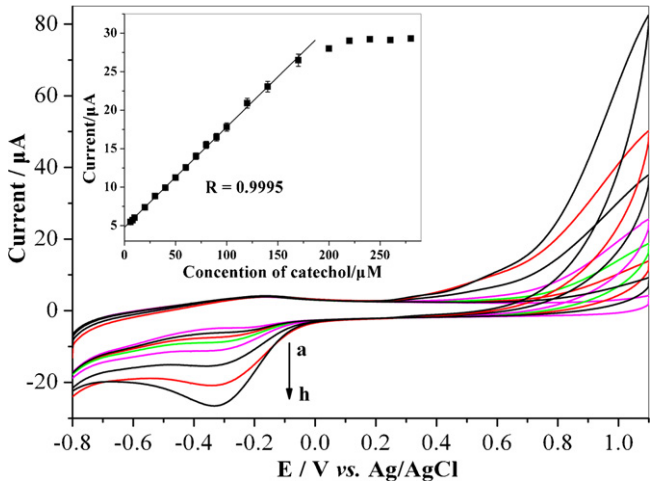

Fig. 5. CVs of the $(LDH/HB/LDH/HRP)_2$ UTF modified electrode in 0.1 M PBS (pH 7.0) with the presence of different concentration of catechol (from a to h: 0, 10, 20, 30, 50, 80, 120 and 170 μM). Scan rate: 0.1 V s^{-1}. Inset: plot of catalytic peak current *vs.* catechol concentration.

$$\text{Heme–Fe(III)} + \text{catechol} + e^- \rightarrow \text{Heme–Fe(II)} + \text{catechol}* \quad (1)$$

$$\text{Heme–Fe(II)} \rightarrow \text{Heme–Fe(III)} + e^- \quad (2)$$

$$\text{catechol}* + e^- \rightarrow \text{catechol} \quad (3)$$

4. Conclusions

A bi-proteinic biosensor has been successfully fabricated based on the alternate assembly of HB and HRP molecules with LDH nanosheets *via* the LBL technique. Structural characterizations show that the $(LDH/HB/LDH/HRP)_n$ UTFs exhibit long range stacking order resulted from a superlattice nanostructure, in which the protein molecule maintain its native structure and form a monolayer arrangement in the LDH gallery. A stable direct electrochemical redox behavior was observed for the $(LDH/HB/LDH/HRP)_2$ modified electrode, owing to the favorable microenvironment imposed by the LDH nanosheets. Based on the synergistic effect of the two proteins, the modified electrode exhibits remarkable electrocatalytic activity towards oxidation of catechol with a wide linear response range, low detection limit, high stability and reproducibility. The methodology reported in this work can be conveniently extended to fabricate other bi-enzymatic biosensors.

Acknowledgments

This project was supported by the National Natural Science Foundation of China, the 111 Project (Grant No. B07004), the 973 Program (Grant No. 2009CB939802) and the Fundamental Research Funds for the Central Universities (Grant No. ZZ0908).

Appendix A. Supplementary data

Supplementary data associated with this article can be found, in the online version, at doi:10.1016/j.bios.2010.07.045.

References

Boclair, J.W., Braterman, P.S., 1999. Chem. Mater. 11, 298–302.
Cao, Z.J., Jiang, X.Q., Xie, Q.J., Yao, S.Z., 2008. Biosens. Bioelectron. 24, 222–227.
Chen, H., Mousty, C., Cosnier, S., Silveira, C., Moura, J.J.G., Almeida, M.G., 2007. Electrochem. Commun. 9, 2240–2245.
Chen, X., Fu, C.L., Wang, Y., Yang, W.S., Evans, D.G., 2008. Biosens. Bioelectron. 24, 356–361.
Delvaux, M., Walcarius, A., Demoustier-Champagne, S., 2005. Biosens. Bioelectron. 20, 1587–1594.
Fogg, A.M., Freij, A.J., Parkinson, G.M., 2002. Chem. Mater. 14, 232–234.
Fogg, A.M., Green, V.M., Harvey, H.G., O'Hare, D., 1999. Adv. Mater. 11, 1466–1469.
Geraud, E., Prevot, V., Forano, C., Mousty, C., 2008. Chem. Commun. 13, 1554–1556.
Han, J.B., Lu, J., Wei, M., Wang, Z.L., Duan, X., 2008. Chem. Commun. 41, 5188–5190.
Khan, A.I., Lei, L., Norquist, A.J., O'Hare, D., 2001. Chem. Commun. 22, 2342–2343.
Kim, G.-Y., Shim, J., Kang, M.-S., Moon, S.-H., 2008. J. Environ. Monit. 10, 632–637.

Leroux, F., Aranda, P., Besse, J.-P., Ruiz-Hitzky, E., 2003. Eur. J. Inorg. Chem. 6, 1242–1251.
Leroux, F., Gachon, J., Besse, J.-P., 2004. J. Solid State Chem. 177, 245–250.
Li, L., Ma, R.Z., Ebina, Y., Iyi, N., Sasaki, T., 2005. Chem. Mater. 17, 4386–4391.
Liu, Z.P., Ma, R.Z., Osada, M., Iyi, N., Ebina, Y., Takada, K., Sasaki, T., 2006. J. Am. Chem. Soc. 128, 4872–4880.
Liu, A.H., Wei, M.D., Honma, I., Zhou, H.S., 2005. Anal. Chem. 77, 8068–8074.
Lu, X.B., Zhang, Q., Zhang, L., Li, J.H., 2006. Electrochem. Commun. 8, 874–878.
Luo, Y.P., Tian, Y., Rui, Q., 2009. Chem. Commun. 21, 3014–3016.
Maaref, A., Barhoumi, H., Rammah, M., Martelet, C., Jaffrezic-Renault, N., Mousty, C., Cosnier, S., 2007. Sens. Actuators B 123, 671–679.
Ma, R., Takada, K., Fukuda, K., Iyi, N., Bando, Y.S., Sasaki, T., 2007. Angew. Chem. Int. Ed. 120, 92–95.
Ma, R.Z., Liu, Z.P., Li, L., Iyi, N., Sasaki, T., 2006. J. Mater. Chem. 16, 3809–3813.
Macha, S.M., Fitch, A., 1998. Mikrochim. Acta 128, 1–18.
Marko-Varga, G.C., EmnCus, J., Got-ton, L., Sweden, L., Ruzgas, T., Lithuania, V., 1995. TrAC, Trends Anal. Chem. 14, 319–328.
Mousty, C., Kaftan, O., Prevot, V., Forano, C., 2008. Sens. Actuators B 133, 442–448.
Ruzgas, T., EmnCus, J., Gorton, L., Marko-Varga, G., 1995. Anal. Chim. Acta 311, 245–253.
Shervedani, R.K., Mehrjardi, A.H., Zamiri, N., 2006. Bioelectrochemistry 69, 201–208.
Shi, G.Y., Sun, Z.Y., Liu, M.C., Zhang, L., Liu, Y., Qu, Y.H., Jin, L.T., 2007. Anal. Chem. 79, 3581–3588.
Shi, L.X., Lu, Y.X., Sun, J., Zhang, J.C., Sun, Q., Liu, J.Q., Shen, J.C., 2003. Biomacromolecules 4, 1161–1167.
Shutava, T.G., Kommireddy, D.S., Lvov, Y.M., 2006. J. Am. Chem. Soc. 128, 9926–9934.
Sun, J.M., Zhang, H., Tian, R.J., Ma, D., Bao, X.H., Su, D.S., Zou, H.F., 2006. Chem. Commun. 12, 1322–1324.
Tortajada, M., Ramón, D., Beltránd, D., Amorós, P., 2005. J. Mater. Chem. 15, 3859–3868.
Wang, B., Zhang, J.J., Pan, Z.Z., Tao, X.Q., Wang, H.S., 2009. Biosens. Bioelectron. 24, 1141–1145.
Williams, G.R., O'Hare, D., 2006. J. Mater. Chem. 16, 3065–3074.
Xiong, H.Y., Chen, T., Zhang, X.H., Wang, S.F., 2007. Electrochem. Commun. 9, 2671–2675.
Xu, Z.P., Braterman, P.S., 2007. J. Phys. Chem. C 111, 4021–4026.
Yan, D.P., Lu, J., Wei, M., Han, J.B., Ma, J., Li, F., Evans, D.G., Duan, X., 2009. Angew. Chem. Int. Ed. 48, 3073–3076.
Yang, S.M., Chen, Z.C., Jin, X., Lin, X.F., 2006. Electrochim. Acta 52, 200–205.
Zeng, X.D., Li, X.F., Liu, X.Y., Liu, Y., Luo, S.L., Kong, B., Yang, S.L., Wei, W.Z., 2009. Biosens. Bioelectron. 25, 896–900.
Zhang, Q., Zhang, L., Liu, B., Lu, X.B., Li, J.G., 2007. Biosens. Bioelectron. 23, 695–700.
Zhao, W., Xu, J.J., Shi, C.G., Chen, H.Y., 2005. Langmuir 21, 9630–9634.
Zhou, Y.L., Hu, N.F., Zeng, Y.H., Rusling, J.F., 2007. Electrochem. Commun. 9, 2671–2675.
Zhu, W., An, Y.R., Luo, X.M., Wang, F., Zheng, J.H., Tang, L.L., Wang, Q.J., Zhang, Z.H., Zhang, W., Jin, L.T., 2009. Chem. Commun. 19, 2682–2684.